

# A Unified Transformer Framework for Group-based Segmentation: Co-Segmentation, Co-Saliency Detection and Video Salient Object Detection

Yukun Su, Jingliang Deng, Ruizhou Sun, Guosheng Lin, and Qingyao Wu

**Abstract**—Humans tend to mine objects by learning from a group of images or several frames of video since we live in a dynamic world. In the computer vision area, many researches focus on co-segmentation (CoS), co-saliency detection (CoSD) and video salient object detection (VSOD) to discover the co-occurrent objects. However, previous approaches design different networks on these similar tasks separately, and they are difficult to apply to each other, which lowers the upper bound of the transferability of deep learning frameworks. Besides, they fail to take full advantage of the cues among inter- and intra-feature within a group of images. In this paper, we introduce a unified framework to tackle these issues, term as UFO (Unified Framework for Co-Object Segmentation). Specifically, we first introduce a transformer block, which views the image feature as a patch token and then captures their long-range dependencies through the self-attention mechanism. This can help the network to excavate the patch structured similarities among the relevant objects. Furthermore, we propose an intra-MLP learning module to produce self-mask to enhance the network to avoid partial activation. Extensive experiments on four CoS benchmarks (PASCAL, iCoseg, Internet and MSRC), three CoSD benchmarks (Cosal2015, CoSOD3k, and CocA) and four VSOD benchmarks (DAVIS<sub>16</sub>, FBMS, ViSal and SegV2) show that our method outperforms other state-of-the-arts on three different tasks in both accuracy and speed by using the same network architecture, which can reach 140 FPS in real-time. Code is available at <https://github.com/suyukun666/UFO>

**Index Terms**—Co-object, Long-range Dependency, Transformer, Activation.

## I. INTRODUCTION

**O**BJECT segmentation [1], [2], [3] and detection [4], [5] are the core tasks in computer vision. In our real world, the continuous emergence of massive group-based data and dynamic multi-frame data make deep learning more in the direction of human vision. As a result, more and more studies focus on co-segmentation (CoS) [6], [7], co-saliency detection (CoSD) [8], [9] and video salient object detection (VSOD) [10], [11]. Among them, these tasks all share the common objects with the same attributes given a group of relevant images or within several adjacent frames in the video. They all essentially aim to discover and segment the co-occurrent object by imitating the human vision system.

However, as shown in Fig 1 top, previous methods tend to design different networks on these tasks in isolation, which may

Y. Su, J. Deng, R. Sun and Q. Wu are with the School of Software Engineering, South China University of Technology, Guangzhou 510640, China, E-mail: suyukun666@gmail.com.

Y. Su and G. Lin is with the School of Computer Science and Engineering, Nanyang Technological University, Singapore.

G. Lin and Q. Wu are the corresponding authors.

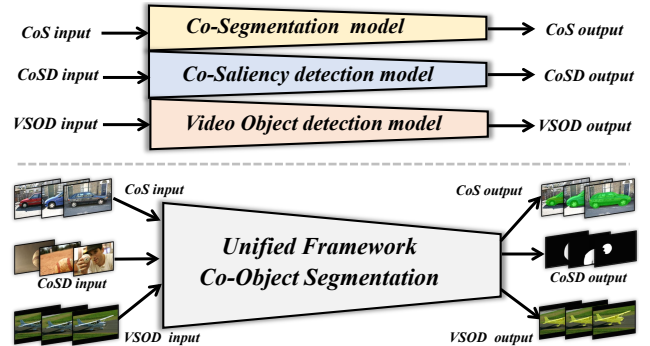


Fig. 1: The main purpose of our proposed framework. The co-object images can be fed into our network to yield the accurate masks in real-time using the same architecture.

lower the upper bound on the ease of usage of deep learning frameworks. Besides, the transferability and applicability of these methods are relatively poor. For example, some of the CoS [6], [12], CoSD [13], [8] and VSOD methods [10], [11] are well-trained on the same dataset [14], [15], they fail to achieve comparable performance on all benchmarks but only their task-targeted benchmarks. This illustrates that there may exist some limitations in previous approaches. To be specific, most of the co-object segmentation and saliency detection networks are based on matching strategies [16], [17], which enable the network to extract and propagate the feature representation not only to express the images individual properties but also reflect the relevance and interaction among group-based images. Some recent works [18], [6] utilize spectral clustering [19] to mine the corresponding object regions. However, such methods are unstable and they are deeply dependent on the upper stream extracted features. Some researches [8], [20] adopt distance measure metric [21], [22] to model the relationship among image pixels, but they can only handle the pair-wise information and it is cumbersome to address group-wise relationships. Some others, like [9], [13] try to use the CNN-based attention technique to establish the relationships among group-based images. However, convolution operations produce local receptive fields and experience difficulty to capture long-range feature dependencies among pixels, which may affect the learning representation of co-object regions. Furthermore, some of the VSOD approaches [11], [23] capture the pair-wise feature between frames with the help of optical flow [24], which greatly increases the network running cost and reduces

the convenience of using the networks.

To this end, we design a unified framework as shown in Fig 1 bottom, term as **UFO (Unified Framework for Co-Object Segmentation)**, to jointly address the aforementioned drawbacks. Specifically, to better reflect the relationships among group-based images, we first introduce a transformer block to insert into our network. It splits the image feature as a patch token and then captures their global dependency thanks to the self-attention mechanism and Multilayer Perceptron (MLP) structure. This can help the network learn complex spatial features and reflect long-range semantic correlations to excavate the patch structured similarities among the relevant objects. The inherent global feature interaction capability of the visual transformer [25] frees us from the computationally expensive similarity matrices as some previous methods [6]. Therefore, our method can achieve real-time performance. In addition to improving inter-collaboration in group-based images, we also propose an intra-MLP learning module to enhance the single image. As it is common that the encoder of the network only focuses on the most discriminative part of the objects [26], in order to avoid partial activation, we add the intra-MLP operation to produce global receptive fields. For each query pixel, it will match with its top- $K$  potentially corresponding pixels, which can help the network learn divergently. Then we produce the self-masks and add them to the decoder to enhance the network. Finally, extensive experiments on four CoS benchmarks (*i.e.*, PASCAL, iCoseg, Internet and MSRC), three CoSD benchmarks (*i.e.*, Cosal2015, CoSOD3k, and CocA) and four VSOD benchmarks (*i.e.*, DAVIS<sub>16</sub>, FBMS, ViSal and SegV2) demonstrate the superiority of our approach and it can outperform the state-of-the-arts in both accuracy and speed by using the same network architecture.

The main contributions of our paper are the following:

- We propose a unified framework for group-based image co-object segmentation (**UFO**). To the best of our knowledge, we take the early attempt to complete three different tasks (co-segmentation, co-saliency detection, video salient object detection) using the same network architecture without using additional prior.
- We introduce the transformer block to capture the feature long-range dependencies among group-based images through the self-attention mechanism. Besides, we design an intra-MLP learning module to avoid partial activation to further enhance the network.
- Experiments on four CoS benchmarks, three CoSD benchmarks, and four VSOD benchmarks in different tasks show the effectiveness of our proposed method. It can achieve the new state-of-the-art performance and reach 140 FPS in real-time.

## II. RELATED WORK

**Co-Segmentation (CoS).** Co-Segmentation is introduced by Rother *et al.* [27], which aims to segment the common objects in pair images. Early conventional works like Gabor filters [28] and SIFT [29] try to extract low-level image features and then detect image foreground. As deep learning recently emerges and demonstrates the success in many computer vision applications,

more and more recent studies adopt deep visual features to train object co-segmentation. Chen *et al.* [30] and Li *et al.* [31] first propose the siamese fully convolutional network to solve the object co-segmentation task with a mutual correlation layer. However, both of them can not achieve satisfactory performance and they can only deal with pair-wise images. Later, Li *et al.* [12] and Zhang [7] *et al.* both propose group-wise networks using LSTM [32]. Although they can improve the performance, they are computationally expensive because of the serial structure of recurrent neural network. Besides, training such methods will have a risk such as forgetting historical information. More recently, Chen *et al.* [33] proposes a matching strategy to jointly complete semantic matching and object Co-segmentation. Such a method is targeted for bipartite matching, which is hard to apply to group-based segmentation. Zhang [6] later designs a spatial-semantic network with sub-cluster optimizing. The cluster results are deeply dependent on the upper extracted features and thus, it may make the training unstable.

**Co-Saliency Detection (CoSD).** Co-Saliency Detection is similar to Co-Segmentation. The main difference between them lies in that salient detection mimics the human vision system to distinguish the most visually distinctive regions [34], [8]. Previous standard methods [35], [36], [37] try to use hand-crafted cues or super-pixels prior to discover the co-saliency from the images. Later, researchers pay more attention to explore the deep-based models in a data-driven manner in various ways, *i.e.*, co-category semantic fusion [38], [6], gradient-induced [34] and CNN-based self-attention [9], [13], *etc.* However, these works do not fully consider the global correlation among the group-based images since the convolution local receptive fields. Some recent works [39], [18] exploit GCN to solve the non-local problem in CNN. However, in these methods, a large number of similarity matrices and adjacency matrices need to be constructed for the graph, which will slow down the networks and are computational costly. Zhang *et al.* [8] proposes to use GW distance [40] to build the dense correlation volumes for image pixels. However, it has to select a target image and source images, which ignore the attention on the target image itself. Moreover, the distance metric problem in the network needs a sub-solver to optimize. This will cost more time for matching. Compared to it, for a query patch, our transformer block can capture the relationships of both inter-pixel within group-based images and intra-pixel within a single image, which can model the global long-range semantic correlations rapidly.

**Video Salient Object Detection (VSOD).** In video salient object detection, since the content of each frame is highly correlated, it can be considered whose purpose is to capture long-range feature information among the adjacency frame. Traditional methods [41], [42], [43], [44] are usually based on classic heuristics in image salient object detection area. Subsequently, some works [45], [46] rely on 3D-convolution to capture the temporal information. However, the 3D convolution operation is very time-costly. In recent, more and more schemes [11], [47], [43] propose to combine optical flow [24] to locate the representative salient objects in video frames.

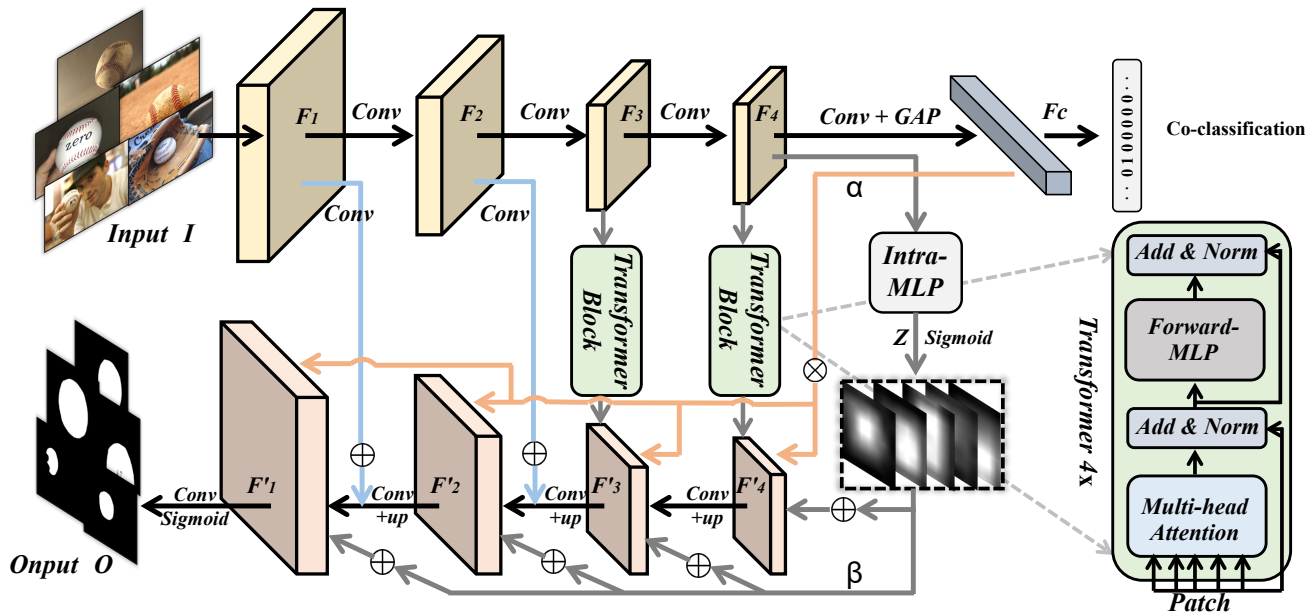


Fig. 2: **The pipeline of our proposed method.** The given group-based input images  $\mathcal{I}$  are first fed into the encoder, yielding the multi-scale feature maps  $F$ . Then we employ transformer blocks (see Fig 3 for more details) on the last two layers to capture the images long-range correlations to model the patch structured similarities among the relevant objects, which will output the updated co-attention layers  $F'$ . In addition, the last layer feature are passed through a classification sub-network and an intra-MLP module. The former exploits the co-category associated information and the latter produce the self-masks. Finally, they are combined with the updated co-attention layers to enhance the co-object semantic-aware regions in the pyramid network structure-like decoder to produce the output  $\mathcal{O}$ .

In practical usage, obtaining additional prior information such as optical flow will make the deep learning network inconvenient, which can not be a real sense of end-to-end network. More recently, some approaches exploit attention-based mechanisms to better establish the pair-wise relation in the area in consecutive frames. Fan *et al.* [48] and Gu *et al.* [10] propose a visual-attention-consistent module and a pyramid constrained self-attention block to better capture the temporal dynamics cues, respectively. However, these models can not transfer well to the above tasks. Therefore, in this paper, we propose a unified framework to solve these problems in a more comprehensive way.

### III. METHODOLOGY

#### A. Architecture Overview

Given a group of  $N$  images  $\mathcal{I} = \{I^n\}_{n=1}^N$  that contain co-occurrent objects, our target is to produce the accurate masks output  $\mathcal{O} = \{O^n\}_{n=1}^N$  that represent the share foregrounds. To achieve this goal, we propose a unified framework for co-object segmentation (UFO). As depicted in Fig 2, the overall architecture of our network is based on an encoder (*i.e.*, VGG16 [49]) to extract multi-scale layer features  $\{F_1, F_2, F_3, F_4\}$ . The transformer blocks in the last two layers are responsible for matching the co-objects similarities in multi-resolution feature maps, producing the enhanced co-attention maps  $\{F'_3, F'_4\}$ . Besides, the intra-MLP learning representation and the co-category semantic guidance are leveraged to combine with the updated maps in the decoder to enhance co-object

regions. Specifically, the co-category embedding response  $\alpha$  is multiplied by the decoder features, and the intra self-masks  $\beta$  are added to the decoder features. The encoder-decoder structure in our network is similar to the feature pyramid network [50], whose top-level features are fused by upsampling with low-level features in skip connection. Furthermore, the input of our network can be not only a group of images with relevant objects but also a multi-frame video.

#### B. Transformer Block

**Preliminaries.** In visual transformer [25], in order to handle 2D images, an input image will be divided into a sequence of flattened 2D patches. The transformer uses a constant latent vector size  $D$  in all its layers for each token embedding. Each layer consists of a multi-head self-attention layer and a Multilayer Perceptron (MLP) operation. Compared to other group-based image matching strategies and feature extraction methods, we consider that transformer block has two main advantages: (1) Although transformer is not specially designed for image matching, it has the intrinsic ability to capture global cues across all input patch tokens, which we have mentioned in Sec.II. (2) The transformer parallelizes the patch tokens, which is faster than some of the serial processing methods and can achieve real-time performance.

**Semantic Patch Collaboration.** The detailed workflow of the transformer block is shown in Fig 3 left. Since we employ transformer blocks both on  $F_3$  and  $F_4$  layers in multi-resolution feature maps, for simplicity, we omit  $F_3$  in the

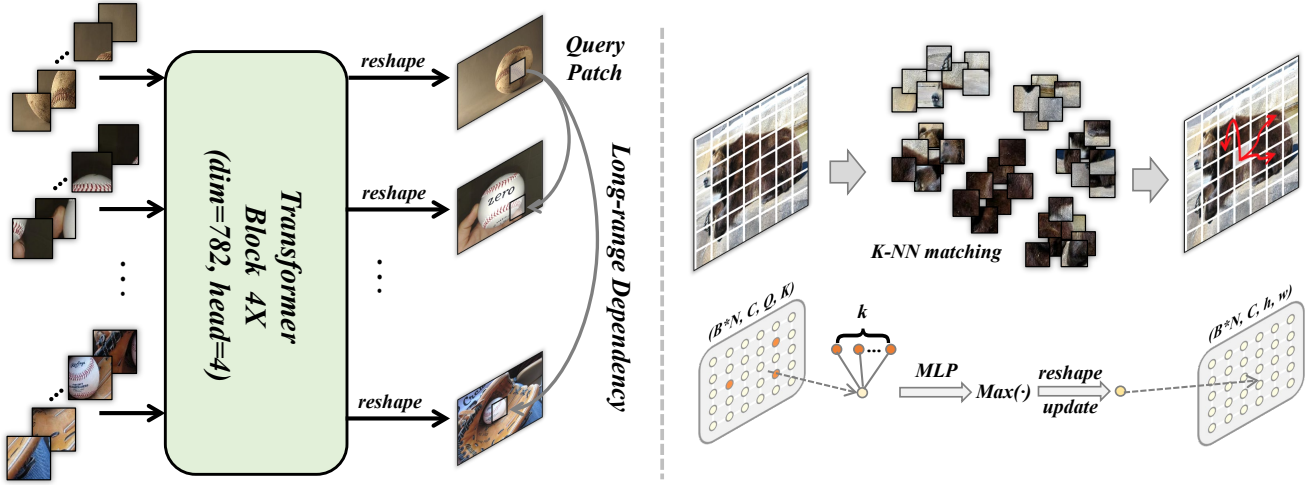


Fig. 3: **Detailed illustration of the transformer block and the intra-MLP learning module.** Left: A group of images  $\mathcal{I}$  are reshaped into patches. The transformer encoder will output the enhanced patch embeddings implemented by the multi-head MLP. We then reshape all the patches into image-like feature maps. Right: For each query image feature patch, it will match with its top- $K$  potentially corresponding patches. Then, it will be updated by aggregating different sub-region representations using MLP operation.

following. Concretely, we first reshape  $F_4 \in \mathbb{R}^{B*N*C*h*w}$  ( $w$  and  $h$  denote the spatial size of the feature map,  $C$  is the feature dimension,  $B$  and  $N$  denote the batch size and group size, respectively) into a sequence flattened patch tokens  $T \in \mathbb{R}^{B*C*P}$ , where  $P = N * h * c$ . All these tokens are then fed into the transformer blocks and yield the updated patch embeddings  $T'$  by:

$$T' = \text{Multi-Head}(\text{MLP}(T)), \quad (1)$$

where the trainable linear projection maps the patches from the original  $C$  dimensions to  $D$  dimensions, and back to  $C$  dimensions. Afterward, we reshape  $T'$  back into an image-like feature map  $F'_4 \in \mathbb{R}^{B*N*C*h*w}$ . Due to the inductive bias [51] of convolution, the features extracted by the encoder convolution layers are not sensitive to the global location of features but only care about the existence of decisive features. The proposed transformer block can complement convolution and enhance the representations of the global co-object regions.

**What it learns?** Fig 4 shows what the transformer blocks learn (the output is from  $F'_3$ ). As can be seen in the 3<sup>rd</sup> row, the corresponding image patches of the co-object regions are highly activated after operated by the transformer block comparing to the 2<sup>nd</sup> row, which illustrates that the attention mechanism in transformer projection function can adaptively pay attention to the targeted areas and assign more weights to capture the global cues from all the images. In addition, we also visualize the query attention of the picked image patch (*i.e.*, the endpoints of the “banana” and the “head” of the penguin) to show what it will match. The qualitative visualizations in the 3<sup>rd</sup> row further validate that the transformer block can help the network model the long-range dependencies among different location pixels.

### C. Intra-MLP module

In addition to the image inter-collaboration, we also propose an intra-MLP learning module to activate more self-object areas within a single image. As shown in Fig 3 right, the top layer feature map from the encoder are viewed as different patches. We consider that different patches will not just match with their nearest ones as in CNN (local receptive fields) since the long-distance patch features may share some similar responses (*i.e.*, color and texture). Motivated by this, we can fuse the non-local semantic information to improve the object learning representation. Concretely, the top layer feature  $F_4 \in \mathbb{R}^{B*N*C*h*w}$  is reshaped into  $\bar{F}_4 \in \mathbb{R}^{B*N*C*Q}$ , where  $Q = h * w$  is the number of patches. We then construct a matrix  $M$  that represents the similarity of each patch within a single image. Specifically, we use  $\ell_2$ - distance to measure the relationship between the two arbitrary patches. Since we use normalized channel features, by removing the constant, the matrix  $M \in \mathbb{R}^{B*N*Q*Q}$  can be formulated as:

$$M = \bar{F}_4^T \bar{F}_4. \quad (2)$$

To avoid the patches match with themselves, the diagonal elements of the matrix are set to  $-INF$ . For each query patch, we perform  $KNN$  operation on the matrix to select its potentially corresponding target patches. Then, it will output a tensor in  $Q \times K$  shape, which indicates the patches along with their top- $K$  semantically related patches. After that, we can acquire the  $\hat{F}_4 \in \mathbb{R}^{B*N*C*Q*K}$ , and then we perform MLP with  $MAX(\cdot)$  operations on it to get the updated feature  $Z \in \mathbb{R}^{B*N*C*Q}$  as:

$$Z = \text{MAX}(\text{MLP}(\hat{F}_4)), \quad (3)$$

where  $MAX$  is the element-wise maximum operation. This guarantees that the combination of MLP and symmetric

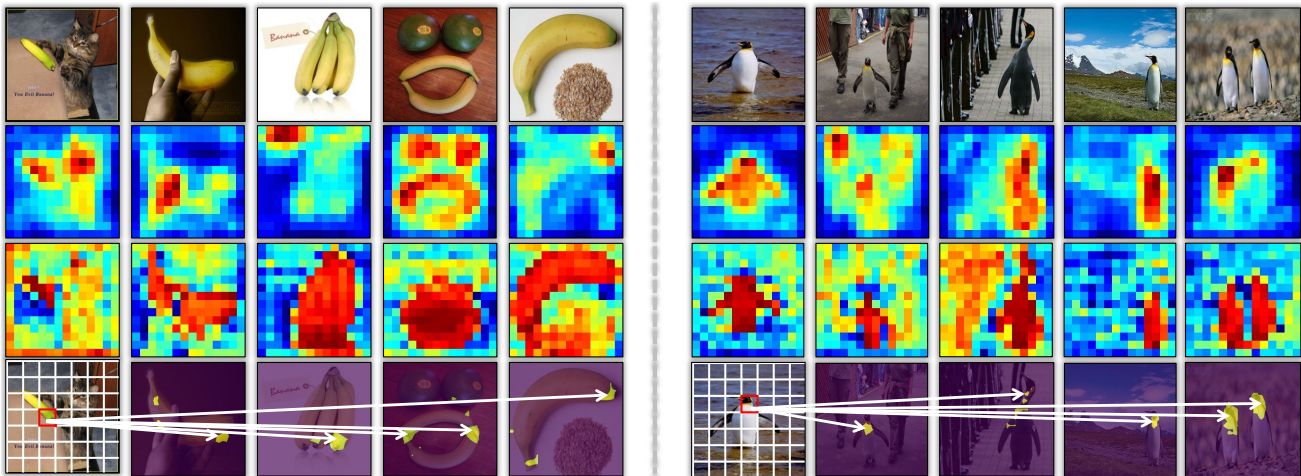


Fig. 4: **Analysis of the transformer block.** The 1<sup>st</sup> row: original group-based images input, note that we deliberately pick some hard examples with complex backgrounds and multi-objects. The 2<sup>nd</sup> row: the responded maps before transformer. The 3<sup>rd</sup> row: the responded maps of the patch tokens after transformer. The 4<sup>th</sup> row: the corresponding attention maps of the selected patches (marked with red rectangles in the query images).

function can arbitrarily approximate any continuous set function [52]. The purpose of this step is to combine the target feature with its top- $K$  features appearance change information and learn through the perceptron. Finally, we reshape  $Z \in \mathbb{R}^{B*N*C*Q}$  back into  $Z \in \mathbb{R}^{B*N*C*h*w}$  and employ  $Sigmoid(\cdot)$  to  $Z$  to yield the self-masks  $\beta$ .

#### D. Network Training

Moreover, since the co-category information can also be used, the top layer  $F_4$  is thus passed through a convolutional layer as [38], [6], following a  $GAP$  layer to yield a vector  $\alpha$ . And the  $FC$  layer classifies the embedding  $\alpha$  to predict the co-category labels  $\hat{y}$ . Then we combine both the  $\alpha$  and self-masks  $\beta$  to enhance the decoder layer in a conditional normalization way [53] modulated with learned scale and bias. Specifically, the variables  $\alpha$  are the learned scale modulation parameters that exclude the distractors in co-objects regions by using the rich semantic-aware clues. The variables  $\beta$  serve as the bias parameters complement and highlight the object targets by endowing spatial-aware information. The decoder leverages the skip connection structure to fuse the low-resolution layer features from the encoder. Ultimately, it outputs the co-object masks.

**Objective Function.** Firstly, classification loss is used to update the gradient propagation for the semantic information as:

$$\mathcal{L}_{cls} = \mathcal{L}_{ce}(y, \hat{y}), \quad (4)$$

where  $\mathcal{L}_{ce}$  is the cross-entropy loss,  $y$  is the ground-truth class label and  $\hat{y}$  is the prediction. Besides, the Weighted Binary Cross-Entropy (WBCE) loss for pixel-wise segmentation is also adopted as:

$$\begin{aligned} \mathcal{L}_{wbce} = & -\frac{1}{HW} \sum_{i=1}^H \sum_{j=1}^W \gamma G(i, j) \log(P(i, j)) \\ & - (1 - \gamma)(1 - G(i, j)) \log(1 - P(i, j)), \end{aligned} \quad (5)$$

where  $H$  and  $W$  denote the height and width of the image.  $G(i, j) \in \{0, 1\}$  is the ground truth mask and  $P(i, j)$  is the predicted probability.  $\gamma$  is the ratio of all positive pixels over all pixels in images. Moreover, similar to [54], [9], IoU loss is also widely used to evaluate segmentation accuracy as follows:

$$\mathcal{L}_{iou} = 1 - \frac{\sum_{i=1}^H \sum_{j=1}^W P(i, j)G(i, j)}{\sum_{i=1}^H \sum_{j=1}^W [P(i, j) + G(i, j) - P(i, j)G(i, j)]}. \quad (6)$$

The whole framework is optimized by integrating all the aforementioned loss functions in an end-to-end manner:

$$\mathcal{L}_{total} = \mathcal{L}_{cls} + \mathcal{L}_{wbce} + \mathcal{L}_{iou}. \quad (7)$$

## IV. EXPERIMENTS

**Datasets.** Following [7], [6], we conduct experiments on four co-segmentation benchmarks including: PASCAL-VOC [55], iCoseg [56], Internet [29] and MSRC [57]. Among them, PASCAL-VOC is the most challenging dataset with 1,037 images of 20 categories. For co-saliency detection, our method is evaluated on the three largest and most challenging benchmark datasets, including Cosal2015 [58], CoCA [34], and CoSOD3k [59]. The CoSOD3k is the largest evaluation benchmark for real-world co-saliency proposed recently, which has a total of 160 categories with 3,316 images. And all of them contain multiple objects against a complex background. In terms of video salient object detection, we benchmark our method on four public datasets, *i.e.*, DAVIS<sub>16</sub> [60] (30 videos training and 20 videos validation), FBMS [61] (29 training

Baseline	$\alpha$	$\beta$	Trans	PASCAL		iCoseg	
				$\mathcal{P}$	$\mathcal{J}$	$\mathcal{P}$	$\mathcal{J}$
✓				81.2	36.8	85.2	52.8
✓	✓			92.4	68.1	95.3	87.9
✓		✓		82.9	37.6	86.0	53.3
✓			✓	92.1	69.5	95.6	86.4
✓	✓	✓		92.5	68.6	95.3	88.1
✓	✓		✓	95.0	72.7	96.9	89.8
✓		✓	✓	92.8	69.6	95.9	87.1
✓	✓	✓	✓	<b>95.4</b>	<b>73.6</b>	<b>97.6</b>	<b>90.9</b>

TABLE I: Analysis of different modules and their combinations.

Transformer		PASCAL		iCoseg	
		$\mathcal{P}$	$\mathcal{J}$	$\mathcal{P}$	$\mathcal{J}$
Block = 2	Head = 2	94.0	71.8	95.9	89.1
	Head = 4	94.2	72.5	96.3	89.4
	Head = 6	94.6	73.0	96.4	89.9
Block = 4	Head = 2	94.8	72.9	97.3	90.4
	Head = 4	95.4	<b>73.6</b>	<b>97.6</b>	<b>90.9</b>
	Head = 6	95.0	73.5	97.5	90.2
Block = 6	Head = 2	95.1	72.9	97.1	90.6
	Head = 4	<b>95.6</b>	72.8	97.3	90.2
	Head = 6	95.0	73.1	97.5	90.4

TABLE II: Analysis of the block and multi-head number in transformer.

videos and 30 testing videos), ViSal [62] (consists of 17 video sequences for testing) and SegV2 [63] (consists of 13 clips for testing).

**Evaluation Metrics.** Two widely used measures, Precision ( $\mathcal{P}$ ) and Jaccard index ( $\mathcal{J}$ ), are used to evaluate the performance of object co-segmentation. For co-saliency detection and video salient object detection, we adopt four evaluation metrics for comparison, including the mean absolute error MAE [64], F-measure  $F_\beta$  [65], E-measure  $E_m$  [66], and S-measure  $S_m$  [67].

**Training Details.** The input image group  $\mathcal{I}$  contains  $N = 5$  images. The mini-batch size is set to  $8 \times N$ . For fair comparisons, we strictly follow the same settings as [34], [9] to use VGG16 [49] as backbone and the images are all resized to  $224 \times 224$  for training and testing unless otherwise stated. We use 4 transformer blocks with 4 multi-heads and  $K$  is set to 4 by default. And the feature dimension of the transformer linear projection function is 782. **(1):** On both co-segmentation (CoS) and co-saliency detection (CoSD) tasks, we follow [38], [13] to use the COCO-SEG [14] for training, which contains 200,000 images belonging to 78 groups. And each image has a manually-labeled binary mask with co-category labels. We leverage the Adam algorithm [68] as the optimization strategy with  $\beta_1 = 0.9$  and  $\beta_2 = 0.999$ . The learning rate is initially set to  $1e-5$  and reduces by a half every 25,000 steps. The whole training takes about 20 hours for total 100,000 steps. **(2):** On video salient detection task (VSOD), the common practice for most methods [10], [11] are first pre-trained on the static saliency dataset. Following this scheme, we first load the weights pre-trained on CoS and CoSD tasks and use DUT [15] dataset to train our network to avoid over-fitting. And then we frozen the co-classification layer since we do not have class labels in VSOD task. Lastly, we train on the training

Method	PASCAL		iCoseg	
	$\mathcal{P}$	$\mathcal{J}$	$\mathcal{P}$	$\mathcal{J}$
$F_3$ only	92.1	69.8	94.6	86.4
$F_4$ only	94.1	72.8	96.2	88.7
$F_3$ and $F_4$	<b>95.4</b>	<b>73.6</b>	<b>97.6</b>	<b>90.9</b>

TABLE III: Analysis of the features from different stages in the encoder.

Method	PASCAL		iCoseg	
	$\mathcal{P}$	$\mathcal{J}$	$\mathcal{P}$	$\mathcal{J}$
Conv	94.8	72.3	96.8	89.7
Non-Local [69]	95.1	72.9	97.2	90.1
<b>Intra-MLP</b>	<b>95.4</b>	<b>73.6</b>	<b>97.6</b>	<b>90.9</b>

TABLE IV: Analysis of different operations for self-masks production.

Method	Time (ms)
Cluster [6]	49.1
Graph [18]	50.2
GW-Distance [8]	>50
<b>Transformer</b>	<b>5.4</b>

TABLE V: Analysis of different methods' matching time cost.

set of DAVIS<sub>16</sub> (30 clips) and FBMS (29 clips) as [11] and it takes about 4 hours. All the experiments are conducted on a RTX 3090 GPU. For all the runtime analysis, we report the results tested on Titan Xp GPU as in [10] for fair comparisons.

#### A. Ablation Studies

To explore each component of our proposed method, we conduct several ablation studies on the CoS (PASCAL-VOC and iCoseg) datasets to demonstrate their effectiveness.

**Comparisons to Baseline:** In Tab I, we investigate the effect of different proposed modules including co-category information  $\alpha$ , intra-MLP masks  $\beta$ , transformer blocks and their combinations. As can be seen, each module can boost the performance of the baseline model to different degrees. Specifically, the proposed transformer block provides the main contributions to help improve the network performances. Whether used alone or in combination with the other two modules, it can outperform other alternatives by a large margin. This illustrates the effectiveness of each component in our framework.

**Settings in Transformer:** Tab II shows the exploration of using different block and multi-head numbers in the transformer. We find that network performance can be improved when increasing the number of blocks and the multi-head attention mechanisms. However, keep increasing both the block and head numbers does not always bring gains to the network (*i.e.*, block = 6), which will also cost much computational resources. We conjecture that large block and multi-head numbers will bring more parameter and redundant information for network



Fig. 5: Qualitative results of our proposed network for “Bus”, “Ballon” and “Bottle” objects.

Method	Backbone	Size	PASCAL		iCoseg		Internet		MSRC	
			$\mathcal{P}$	$\mathcal{J}$	$\mathcal{P}$	$\mathcal{J}$	$\mathcal{P}$	$\mathcal{J}$	$\mathcal{P}$	$\mathcal{J}$
Jerripothula <i>et al.</i> [70] <sub>TMM’2016</sub>	-	-	85.2	45.0	91.9	72.0	88.9	64.0	88.7	71.0
Jerripothula <i>et al.</i> [71] <sub>CVPR’2017</sub>	-	-	80.1	40.0	-	-	-	-	-	-
Wang <i>et al.</i> [72] <sub>TIP’2017</sub>	ResNet50	300 × 300	84.3	52.0	93.8	77.0	-	-	90.9	73.0
Hsu <i>et al.</i> [73] <sub>IJCAI’2018</sub>	VGG16	384 × 384	91.0	60.0	96.5	84.0	92.3	69.8	-	-
Chen <i>et al.</i> [30] <sub>ICCV’2018</sub>	VGG16	512 × 512	-	59.8	-	84.0	-	73.1	-	77.7
Li <i>et al.</i> [31] <sub>ACCV’2018</sub>	VGG16	512 × 512	94.2	64.5	95.1	84.2	93.5	72.6	95.2	82.9
CARNN [12] <sub>ICCV’2019</sub>	VGG19	224 × 224	94.1	63.0	<b>97.9</b>	89.0	<b>97.1</b>	<b>84.0</b>	-	-
SSNM[6] <sub>AAAI’2020</sub>	VGG16	224 × 224	93.7	66.0	96.5	88.0	92.3	67.0	94.3	76.3
Chen <i>et al.</i> [33] <sub>TPAMI’2020</sub>	ResNet101	240 × 240	93.9	61.0	-	-	93.5	70.0	-	-
CycleSegNet[7] <sub>TIP’2021</sub>	ResNet34	512 × 512	<b>96.8</b>	73.6	-	<b>92.1</b>	-	<b>86.2</b>	<b>97.6</b>	<b>89.6</b>
GCoNet†[9] <sub>CVPR’2021</sub>	VGG16	224 × 224	93.5	69.2	96.9	89.7	92.5	70.5	94.0	80.8
CADC†[13] <sub>ICCV’2021</sub>	VGG16	256 × 256	94.1	71.8	97.1	90.2	92.8	71.9	94.4	81.6
<b>UFO (Ours)</b>	VGG16	224 × 224	<b>95.4</b>	<b>73.6</b>	<b>97.6</b>	<b>90.9</b>	<b>93.3</b>	<b>73.7</b>	<b>95.8</b>	<b>83.2</b>
<b>UFO (Ours)</b>	VGG16	256 × 256	<b>96.9</b>	<b>75.7</b>	<b>98.1</b>	<b>92.3</b>	<b>95.2</b>	<b>74.6</b>	<b>97.8</b>	<b>84.3</b>

TABLE VI: Comparisons of our method with the other state-of-the-arts on CoS datasets. † denotes the results using the publicly released code to re-complete. The best two results on each dataset are shown in red and blue.

learning. Therefore, we set both block and multi-head numbers to 4 in our paper.

**Multi-Scale Features:** In our method, we adopt transformer blocks on different top-level layers (*i.e.*,  $F_3$  and  $F_4$ ). Since the low-level (*i.e.*,  $F_1$  and  $F_2$ ) feature maps are large, we do not consider to using them. Tab III reveals that using both the features from the last two layers is better than using the features alone. This indicates that different level features can provide some vital **coarse-to-fine** information in the co-object segmentation task.

**Self-Mask Production:** In Tab IV, we compare our intra-MLP learning module to standard convolution operation and non-local [69]. We can observe that both our method and non-local can improve the performance by accepting more receptive fields to activate object regions compared to the standard convolution. Moreover, although non-local operation can improve the original convolution, it essentially uses some  $1 \times 1$  convolutions to extract features and then reshape and multiply to get the output, which is still worse than our method.

**Matching Time:** We also exhibit the matching time of different methods in co-object regions mining in Tab V. The results illustrate that our proposed method can not only better model co-object long-distance similarities, but also achieve the best performance in speed, which further validates the claim of the advantage of transformer block. More other analysis can be

referred to the supplementary material.

### B. Comparison with State-of-the-arts

**Co-Segmentation.** Tab VI presents the comparisons of our method with other existing CoS methods. Note that there is no standard specification for unifying the various methods on this task, and thus, we point out the respective backbone and input resolution in the table. By using the VGG16 [49] backbone, our framework outperforms all the other methods using the same backbone, even though some of them use a larger input size. Besides, compared to the stronger backbone methods like Chen *et al.* [33] and CycleSegNet [7], we can also achieve relatively comparable performance and even outperforms them. CARNN [12] adopts the VGG19 backbone and achieves the top precision on the Internet dataset. However, it is trained on the full COCO dataset. It contains 9k images belonging to 118 groups, which is much larger than our training set. Furthermore, we also report the performance of some state-of-the-art methods in the co-saliency detection task (*i.e.*, GCoNet [9] and CADC [13]). The results show that our method can also outperform them, which reflects that the transferability of such co-saliency detection methods is poor and they are unsuitable for co-segmentation. In general, our method achieves 5 best results and 2 second-best results on 4 benchmarks, which is competitive. Fig 5 shows some qualitative results and more visualization results can be referred to the supplementary.

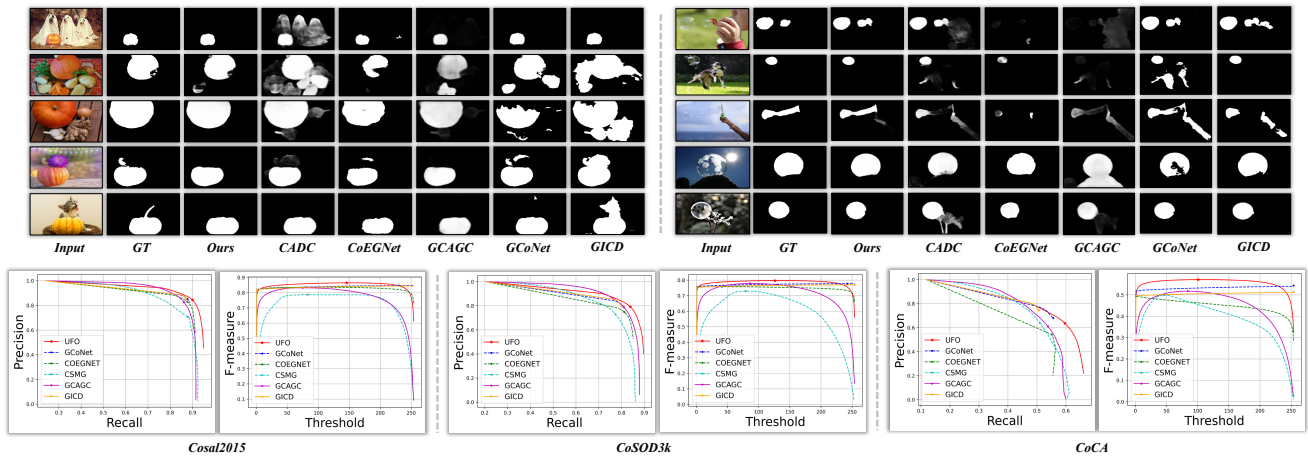


Fig. 6: Qualitative results of our method compared with other state-of-the-art methods and the PR and F-measure curves on three benchmark datasets.

Method	Type	Cosal2015				CoSOD3k				CoCA			
		MAE↓	$S_m$ ↑	$E_m$ ↑	$F_\beta$ ↑	MAE↓	$S_m$ ↑	$E_m$ ↑	$F_\beta$ ↑	MAE↓	$S_m$ ↑	$E_m$ ↑	$F_\beta$ ↑
BASNet[54] <sub>CVPR'2019</sub>	Sin	0.097	0.820	0.846	0.784	0.122	0.753	0.791	0.696	0.195	0.589	0.623	0.397
PoolNet[74] <sub>CVPR'2019</sub>	Sin	0.094	0.820	0.851	0.785	0.120	0.763	0.797	0.704	0.179	0.599	0.631	0.401
EGNet[75] <sub>ICCV'2019</sub>	Sin	0.099	0.818	0.842	0.782	0.119	0.762	0.796	0.703	0.179	0.594	0.637	0.389
SCRN[76] <sub>ICCV'2019</sub>	Sin	0.097	0.814	0.854	0.789	0.118	0.773	0.806	0.717	0.166	0.610	0.658	0.416
RCAN[77] <sub>IJCAI'2019</sub>	Co	0.126	0.779	0.842	0.764	0.130	0.744	0.808	0.688	0.160	0.616	0.702	0.422
CSMG[78] <sub>CVPR'2019</sub>	Co	0.130	0.774	0.818	0.777	0.157	0.711	0.723	0.645	0.124	0.632	0.734	0.503
GICD[34] <sub>ECCV'2020</sub>	Co	0.071	0.842	0.884	0.834	0.089	0.778	0.831	0.743	0.125	0.658	0.701	0.513
SSNM[6] <sub>AAAI'2020</sub>	Co	0.102	0.788	0.843	0.794	0.120	0.726	0.756	0.675	0.116	0.628	0.741	0.482
GCAGC[18] <sub>CVPR'2020</sub>	Co	0.085	0.817	0.866	0.813	0.100	0.785	0.816	0.740	0.111	0.669	0.754	0.523
CoEGNet[59] <sub>ITPAMI'2021</sub>	Co	0.077	0.836	0.882	0.832	0.092	0.762	0.825	0.736	0.106	0.612	0.717	0.493
DeepACG[8] <sub>CVPR'2021</sub>	Co	0.064	0.854	0.892	0.842	0.089	0.792	0.838	0.756	0.102	0.688	0.771	0.552
GCoNet[9] <sub>CVPR'2021</sub>	Co	0.068	0.845	0.887	0.847	0.071	0.802	0.860	0.777	0.105	0.673	0.760	0.544
CADC†[13] <sub>ICCV'2021</sub>	Co	0.064	0.866	0.906	0.862	0.096	0.801	0.840	0.759	0.132	0.681	0.744	0.548
<b>UFO (Ours)</b>	Co	<b>0.064</b>	<b>0.860</b>	<b>0.906</b>	<b>0.865</b>	<b>0.073</b>	<b>0.819</b>	<b>0.874</b>	<b>0.797</b>	<b>0.095</b>	<b>0.697</b>	<b>0.782</b>	<b>0.571</b>

TABLE VII: Comparisons of our method with the other state-of-the-arts on CoSD datasets. “Sin” and “Co” denote single and co-object image saliency object detection methods, respectively. † denotes the results using a larger input size (256 × 256) and copy and paste augmentation strategy. The best two results on each dataset are shown in red and blue.

**Co-Saliency Detection.** Likewise, Tab VII presents the comparisons of our method with other state-of-the-arts in CoSD. Note that all methods use the VGG16 as backbone and the input size is 224 × 224 for fair comparisons unless otherwise specified. We can observe that our framework can also outperform other methods except for two second-best (*i.e.*,  $S_m = 0.860$  in Cosal2015 and  $MAE = 0.073$  in CoSOD3k) results, and all the rest results are ranked the first. It is worth mentioning that unlike some of the previous methods (*i.e.*, GCAGC [18] and CADC [13]), we do not require additional data [15], [93] and data augmentation strategies like Jigsaw in GICD [34] and copy-and-paste in CADC [13] to train the network. Moreover, we visualize the results of some examples (*i.e.*, *pumpkin* and *soap*) with complex backgrounds and some foreground distractors in Fig 6 top. Our method can yield more accurate co-object masks compared to other approaches, which validates the robustness

and effectiveness of our method. Fig 6 bottom shows the PR and the ROC curves of the compared methods, and our curves are higher than the other methods on the three challenging benchmarks.

**Video Salient Object Detection.** We further evaluate our method on VSOD benchmarks. As is shown in Tab VIII, our proposed framework can once again achieve the best results on FBMS, ViSal and SegV2 datasets by using the VGG16 backbone and small input resolution but without optical flow. This shows that our method can effectively extract the object’s spatial appearance information and long-range temporal dependencies, which can also reach 140 FPS for real-time inference. Moreover, the proposed framework is an **unsupervised** VSOD method, which can outperform some **semi-supervised** methods [87], [88], [47] without any bells and whistles. The reason why we fail to achieve the best results

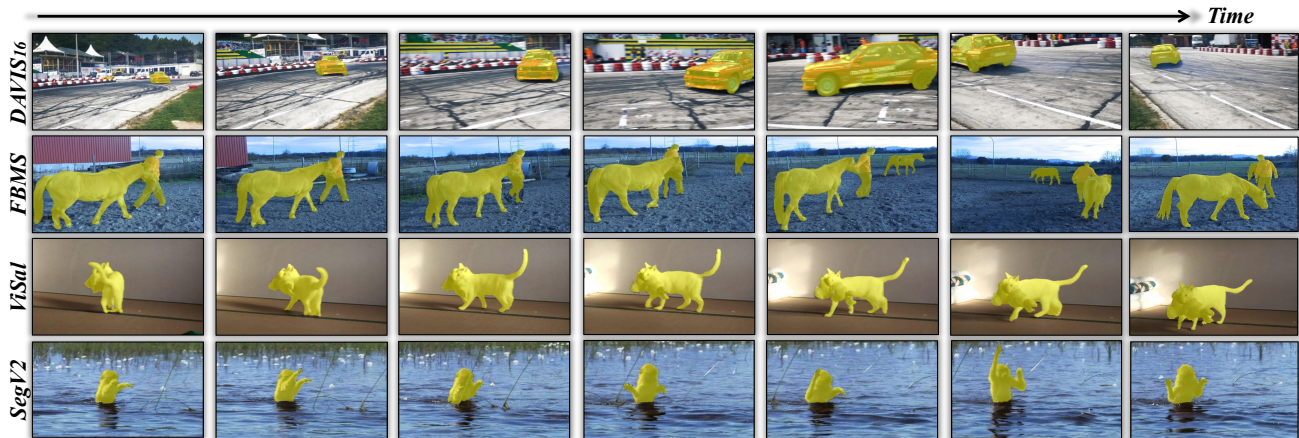


Fig. 7: Qualitative results of our proposed framework on DAVIS, FBMS, ViSal and SegV2 datasets, respectively. More visualizations can be referred to the supplementary material.

Method	Setting	OF	Sup	RT	DAVIS <sub>16</sub>			FBMS			ViSal			SegV2		
					MAE↓	S <sub>m</sub> ↑	F <sub>β</sub> ↑	MAE↓	S <sub>m</sub> ↑	F <sub>β</sub> ↑	MAE↓	S <sub>m</sub> ↑	F <sub>β</sub> ↑	MAE↓	S <sub>m</sub> ↑	F <sub>β</sub> ↑
SCOM[79] <sub>TIP'2018</sub>	DCL[80]	✓	U	38.8	0.048	0.832	0.783	0.079	0.794	0.797	0.122	0.762	0.831	0.030	0.815	0.764
MBNM[81] <sub>ECCV'2018</sub>	DeepLab	✓	U	2.6	0.031	0.887	0.861	0.047	0.857	0.816	0.020	0.898	0.883	0.026	0.809	0.716
PDBM[82] <sub>ECCV'2018</sub>	Res50-473	✗	U	0.05	0.028	0.882	0.855	0.064	0.851	0.821	0.032	0.907	0.888	0.024	0.864	0.800
SRP[83] <sub>TIP'2019</sub>	-	✓	U	17.0	0.070	0.662	0.660	0.134	0.648	0.671	0.092	-	0.752	0.095	-	0.683
MESO[23] <sub>TMM'2019</sub>	-	✓	U	50.3	0.070	0.718	0.660	0.134	0.635	0.618	-	-	-	-	-	-
LTSI[84] <sub>TIP'2019</sub>	VGG16-500	✓	U	1.4	0.034	0.876	0.850	0.087	0.805	0.799	0.027	0.922	0.909	0.028	0.827	0.862
RSE[43] <sub>TCSVT'2019</sub>	-	✓	U	48.2	0.063	0.748	0.698	0.128	0.670	0.652	-	-	-	-	-	-
SSAV[48] <sub>CVPR'2019</sub>	Res50-473	✗	U	0.05	0.028	0.893	0.861	0.040	0.879	0.865	0.020	0.943	0.939	0.023	0.851	0.801
RCR[47] <sub>ICCV'2019</sub>	Res50-448	✓	S	0.04	0.027	0.886	0.848	0.053	0.872	0.859	-	-	-	-	-	-
CAS[85] <sub>TNNLS'2020</sub>	Res50	✗	U	-	0.032	0.873	0.860	0.056	0.856	0.863	-	-	-	0.029	0.820	0.847
PCSA[10] <sub>AAAI'2020</sub>	MobV3-448	✗	U	<b>0.009</b>	0.022	0.902	0.880	0.040	0.868	0.837	0.017	0.946	<b>0.940</b>	0.025	0.865	0.810
DFNet[86] <sub>ECCV'2020</sub>	DeepLab	✗	U	-	<b>0.018</b>	-	0.899	0.054	-	0.833	0.017	-	0.927	-	-	-
FSNet[11] <sub>ICCV'2021</sub>	Res101-352	✓	U	0.08	0.020	<b>0.920</b>	<b>0.907</b>	0.041	0.890	<b>0.888</b>	-	-	-	0.023	0.870	0.772
ReuseVOS†[87] <sub>CVPR'2021</sub>	Res18-480	✗	S	0.02	0.019	0.883	0.865	0.027	0.888	0.884	0.020	0.928	0.933	0.025	0.844	0.832
TransVOS†[88] <sub>Preprint'2021</sub>	Res50-240	✗	S	0.06	<b>0.018</b>	0.885	0.869	0.038	0.867	0.886	0.021	0.917	0.928	0.024	0.816	0.800
<b>UFO (Ours)</b>	VGG16-224	✗	U	<b>0.007</b>	0.036	0.864	0.828	<b>0.028</b>	<b>0.894</b>	<b>0.890</b>	<b>0.011</b>	<b>0.953</b>	<b>0.940</b>	<b>0.022</b>	<b>0.892</b>	<b>0.863</b>
<b>UFO (Ours)</b>	VGG16-224	✓	U	0.01	<b>0.015</b>	<b>0.918</b>	<b>0.906</b>	<b>0.031</b>	<b>0.891</b>	<b>0.888</b>	<b>0.013</b>	<b>0.959</b>	<b>0.951</b>	<b>0.013</b>	<b>0.899</b>	<b>0.869</b>

TABLE VIII: Comparisons of our method with the other state-of-the-arts on VSOD datasets. The majority of the results are borrowed from [11]. *OF* denotes the optical flow. *RT* denotes the runtime (s). “U”: unsupervised method. “S”: semi-supervised method. “Res” denotes ResNet [89], “Mob” denotes Moiblenet [90], and the number behind them is the input resolution. † denotes video segmentation methods trained on DAVIS17 [91] and YouTube-VOS [92] datasets, whose results are acquired from their released code weights. The best two results on each dataset are shown in red, blue.

on the DAVIS is that in some cases the background of co-occurring objects is incorrectly segmented (*e.g.*, foreground: the dancing girl; background: the audience. They all belong to the object of “people”). To alleviate this issue, we combine the flow cues to make our network pay more attention to the foreground moving salient objects and using optical flow in our network is straightforward. Specifically, the images and their corresponding optical flow are passed through the share-encoder at the same time, and the enhanced image features to be fed into subsequent networks can be obtained by multiplying the flow features. More details of the usage of optical flow can be referred to the supplementary material. The quantitative results show that we can achieve new satisfactory results. The performances on FBMS drop a little since the acquired optical flow information are poor. Note that using the optical flow is not our framework’s main purpose and contribution, we recommend

using the multi-frame images alone, which can already achieve state-of-the-art performance in most tasks. Some qualitative results on the 4 VSOD datasets are shown in Fig 7.

## V. CONCLUSION

In this paper, we propose a unified framework for group-based image segmentation, which can conduct co-segmentation, co-saliency detection and video salient object detection tasks. The proposed transformer block and intra-MLP module can both help the network well capture the inter-collaborative and intra-activated information. The competitive results on 11 benchmarks validate the effectiveness of our method. We take an early attempt to unify the deep learning network for different tasks, and we hope this finding will encourage the development of more follow-up research that simplifies the network in other domains.

## ACKNOWLEDGMENT

This work was supported by National Natural Science Foundation of China (NSFC) 61876208, Key-Area Research and Development Program of Guangdong Province 2018B010108002, and the National Research Foundation, Singapore under its AI Singapore Programme (AISG Award No: AISG-RP-2018-003), and the MOE Tier-1 research grants: RG28/18 (S), RG22/19 (S) and RG95/20.

## REFERENCES

- [1] L.-C. Chen, G. Papandreou, I. Kokkinos, K. Murphy, and A. L. Yuille, "DeepLab: Semantic image segmentation with deep convolutional nets, atrous convolution, and fully connected crfs," *IEEE transactions on pattern analysis and machine intelligence*, vol. 40, no. 4, pp. 834–848, 2017. **1**
- [2] L.-C. Chen, Y. Zhu, G. Papandreou, F. Schroff, and H. Adam, "Encoder-decoder with atrous separable convolution for semantic image segmentation," in *Proceedings of the European conference on computer vision (ECCV)*, 2018, pp. 801–818. **1**
- [3] Y. Su, R. Sun, G. Lin, and Q. Wu, "Context decoupling augmentation for weakly supervised semantic segmentation," in *Proceedings of the IEEE/CVF International Conference on Computer Vision*, 2021, pp. 7004–7014. **1**
- [4] A. Bochkovskiy, C.-Y. Wang, and H.-Y. M. Liao, "Yolov4: Optimal speed and accuracy of object detection," *arXiv preprint arXiv:2004.10934*, 2020. **1**
- [5] H. Law and J. Deng, "Cornersnet: Detecting objects as paired keypoints," in *Proceedings of the European conference on computer vision (ECCV)*, 2018, pp. 734–750. **1**
- [6] K. Zhang, J. Chen, B. Liu, and Q. Liu, "Deep object co-segmentation via spatial-semantic network modulation," in *Proceedings of the AAAI Conference on Artificial Intelligence*, vol. 34, no. 07, 2020, pp. 12 813–12 820. **1, 2, 5, 6, 7, 8**
- [7] C. Zhang, G. Li, G. Lin, Q. Wu, and R. Yao, "Cyclesegnet: Object co-segmentation with cycle refinement and region correspondence," *IEEE Transactions on Image Processing*, vol. 30, pp. 5652–5664, 2021. **1, 2, 5, 7**
- [8] K. Zhang, M. Dong, B. Liu, X.-T. Yuan, and Q. Liu, "Deepcag: Co-saliency detection via semantic-aware contrast gromov-wasserstein distance," in *Proceedings of the IEEE/CVF Conference on Computer Vision and Pattern Recognition*, 2021, pp. 13 703–13 712. **1, 2, 6, 8**
- [9] Q. Fan, D.-P. Fan, H. Fu, C.-K. Tang, L. Shao, and Y.-W. Tai, "Group collaborative learning for co-salient object detection," in *Proceedings of the IEEE/CVF Conference on Computer Vision and Pattern Recognition*, 2021, pp. 12 288–12 298. **1, 2, 5, 6, 7, 8**
- [10] Y. Gu, L. Wang, Z. Wang, Y. Liu, M.-M. Cheng, and S.-P. Lu, "Pyramid constrained self-attention network for fast video salient object detection," in *Proceedings of the AAAI conference on artificial intelligence*, vol. 34, no. 07, 2020, pp. 10 869–10 876. **1, 3, 6, 9, 13**
- [11] G.-P. Ji, K. Fu, Z. Wu, D.-P. Fan, J. Shen, and L. Shao, "Full-duplex strategy for video object segmentation," in *Proceedings of the IEEE/CVF International Conference on Computer Vision*, 2021, pp. 4922–4933. **1, 2, 6, 9, 13**
- [12] B. Li, Z. Sun, Q. Li, Y. Wu, and A. Hu, "Group-wise deep object co-segmentation with co-attention recurrent neural network," in *Proceedings of the IEEE/CVF International Conference on Computer Vision*, 2019, pp. 8519–8528. **1, 2, 7**
- [13] N. Zhang, J. Han, N. Liu, and L. Shao, "Summarize and search: Learning consensus-aware dynamic convolution for co-saliency detection," in *Proceedings of the IEEE/CVF International Conference on Computer Vision*, 2021, pp. 4167–4176. **1, 2, 6, 7, 8, 13**
- [14] T.-Y. Lin, M. Maire, S. Belongie, J. Hays, P. Perona, D. Ramanan, P. Dollár, and C. L. Zitnick, "Microsoft coco: Common objects in context," in *European conference on computer vision*. Springer, 2014, pp. 740–755. **1, 6, 13**
- [15] L. Wang, H. Lu, Y. Wang, M. Feng, D. Wang, B. Yin, and X. Ruan, "Learning to detect salient objects with image-level supervision," in *Proceedings of the IEEE conference on computer vision and pattern recognition*, 2017, pp. 136–145. **1, 6, 8, 13**
- [16] J. Ma, X. Jiang, A. Fan, J. Jiang, and J. Yan, "Image matching from handcrafted to deep features: A survey," *International Journal of Computer Vision*, vol. 129, no. 1, pp. 23–79, 2021. **1**
- [17] Y. Liu, L. Zhu, M. Yamada, and Y. Yang, "Semantic correspondence as an optimal transport problem," in *Proceedings of the IEEE/CVF Conference on Computer Vision and Pattern Recognition*, 2020, pp. 4463–4472. **1**
- [18] K. Zhang, T. Li, S. Shen, B. Liu, J. Chen, and Q. Liu, "Adaptive graph convolutional network with attention graph clustering for co-saliency detection," in *Proceedings of the IEEE/CVF conference on computer vision and pattern recognition*, 2020, pp. 9050–9059. **1, 2, 6, 8, 13**
- [19] U. Von Luxburg, "A tutorial on spectral clustering," *Statistics and computing*, vol. 17, no. 4, pp. 395–416, 2007. **1**
- [20] C. Zhang, Y. Cai, G. Lin, and C. Shen, "Deepemd: Few-shot image classification with differentiable earth mover's distance and structured classifiers," in *Proceedings of the IEEE/CVF conference on computer vision and pattern recognition*, 2020, pp. 12 203–12 213. **1**
- [21] J. Solomon, G. Peyré, V. G. Kim, and S. Sra, "Entropic metric alignment for correspondence problems," *ACM Transactions on Graphics (ToG)*, vol. 35, no. 4, pp. 1–13, 2016. **1**
- [22] Y. Rubner, C. Tomasi, and L. J. Guibas, "The earth mover's distance as a metric for image retrieval," *International journal of computer vision*, vol. 40, no. 2, pp. 99–121, 2000. **1**
- [23] M. Xu, B. Liu, P. Fu, J. Li, and Y. H. Hu, "Video saliency detection via graph clustering with motion energy and spatiotemporal objectness," *IEEE Transactions on Multimedia*, vol. 21, no. 11, pp. 2790–2805, 2019. **1, 9**
- [24] E. Ilg, N. Mayer, T. Saikia, M. Keuper, A. Dosovitskiy, and T. Brox, "FlowNet 2.0: Evolution of optical flow estimation with deep networks," in *Proceedings of the IEEE conference on computer vision and pattern recognition*, 2017, pp. 2462–2470. **1, 2, 13**
- [25] A. Dosovitskiy, L. Beyer, A. Kolesnikov, D. Weissenborn, X. Zhai, T. Unterthiner, M. Dehghani, M. Minderer, G. Heigold, S. Gelly *et al.*, "An image is worth 16x16 words: Transformers for image recognition at scale," *arXiv preprint arXiv:2010.11929*, 2020. **2, 3**
- [26] B. Zhou, A. Khosla, A. Lapedriza, A. Oliva, and A. Torralba, "Learning deep features for discriminative localization," in *Proceedings of the IEEE conference on computer vision and pattern recognition*, 2016, pp. 2921–2929. **2**
- [27] C. Rother, T. Minka, A. Blake, and V. Kolmogorov, "Cosegmentation of image pairs by histogram matching—incorporating a global constraint into mrfs," in *2006 IEEE Computer Society Conference on Computer Vision and Pattern Recognition (CVPR'06)*, vol. 1. IEEE, 2006, pp. 993–1000. **2**
- [28] D. S. Hochbaum and V. Singh, "An efficient algorithm for co-segmentation," in *2009 IEEE 12th International Conference on Computer Vision*. IEEE, 2009, pp. 269–276. **2**
- [29] M. Rubinstein, A. Joulin, J. Kopf, and C. Liu, "Unsupervised joint object discovery and segmentation in internet images," in *Proceedings of the IEEE conference on computer vision and pattern recognition*, 2013, pp. 1939–1946. **2, 5**
- [30] H. Chen, Y. Huang, and H. Nakayama, "Semantic aware attention based deep object co-segmentation," in *Asian Conference on Computer Vision*. Springer, 2018, pp. 435–450. **2, 7**
- [31] W. Li, O. Hosseini Jafari, and C. Rother, "Deep object co-segmentation," in *Asian Conference on Computer Vision*. Springer, 2018, pp. 638–653. **2, 7**
- [32] S. Hochreiter and J. Schmidhuber, "Long short-term memory," *Neural computation*, vol. 9, no. 8, pp. 1735–1780, 1997. **2**
- [33] Y.-C. Chen, Y.-Y. Lin, M.-H. Yang, and J.-B. Huang, "Show, match and segment: Joint weakly supervised learning of semantic matching and object co-segmentation," *IEEE Transactions on Pattern Analysis and Machine Intelligence*, vol. 43, no. 10, pp. 3632–3647, 2020. **2, 7**
- [34] Z. Zhang, W. Jin, J. Xu, and M.-M. Cheng, "Gradient-induced co-saliency detection," in *European Conference on Computer Vision*. Springer, 2020, pp. 455–472. **2, 5, 6, 8, 13**
- [35] H. Li, F. Meng, and K. N. Ngan, "Co-salient object detection from multiple images," *IEEE Transactions on Multimedia*, vol. 15, no. 8, pp. 1896–1909, 2013. **2**
- [36] H. Song, Z. Liu, Y. Xie, L. Wu, and M. Huang, "Rgb-d co-saliency detection via bagging-based clustering," *IEEE Signal Processing Letters*, vol. 23, no. 12, pp. 1722–1726, 2016. **2**
- [37] K. R. Jerripothula, J. Cai, and J. Yuan, "Cats: Co-saliency activated tracklet selection for video co-localization," in *European Conference on Computer Vision*. Springer, 2016, pp. 187–202. **2**
- [38] C. Wang, Z.-J. Zha, D. Liu, and H. Xie, "Robust deep co-saliency detection with group semantic," in *Proceedings of the AAAI Conference on Artificial Intelligence*, vol. 33, no. 01, 2019, pp. 8917–8924. **2, 5, 6**
- [39] B. Jiang, X. Jiang, A. Zhou, J. Tang, and B. Luo, "A unified multiple graph learning and convolutional network model for co-saliency estimation," in

- Proceedings of the 27th ACM International Conference on Multimedia*, 2019, pp. 1375–1382. 2
- [40] F. Mémoli, “The gromov–wasserstein distance: A brief overview,” *Axioms*, vol. 3, no. 3, pp. 335–341, 2014. 2
- [41] Y. Wei, F. Wen, W. Zhu, and J. Sun, “Geodesic saliency using background priors,” in *European conference on computer vision*. Springer, 2012, pp. 29–42. 2
- [42] W. Wang, J. Shen, R. Yang, and F. Porikli, “Saliency-aware video object segmentation,” *IEEE transactions on pattern analysis and machine intelligence*, vol. 40, no. 1, pp. 20–33, 2017. 2
- [43] M. Xu, B. Liu, P. Fu, J. Li, Y. H. Hu, and S. Feng, “Video salient object detection via robust seeds extraction and multi-graphs manifold propagation,” *IEEE Transactions on Circuits and Systems for Video Technology*, vol. 30, no. 7, pp. 2191–2206, 2019. 2, 9
- [44] X. Zhou, Z. Liu, C. Gong, and W. Liu, “Improving video saliency detection via localized estimation and spatiotemporal refinement,” *IEEE Transactions on Multimedia*, vol. 20, no. 11, pp. 2993–3007, 2018. 2
- [45] D. Tran, L. Bourdev, R. Fergus, L. Torresani, and M. Paluri, “Learning spatiotemporal features with 3d convolutional networks,” in *Proceedings of the IEEE international conference on computer vision*, 2015, pp. 4489–4497. 2
- [46] S. Mahadevan, A. Athar, A. Oşep, S. Hennen, L. Leal-Taixé, and B. Leibe, “Making a case for 3d convolutions for object segmentation in videos,” *arXiv preprint arXiv:2008.11516*, 2020. 2
- [47] P. Yan, G. Li, Y. Xie, Z. Li, C. Wang, T. Chen, and L. Lin, “Semi-supervised video salient object detection using pseudo-labels,” in *Proceedings of the IEEE/CVF International Conference on Computer Vision*, 2019, pp. 7284–7293. 2, 8, 9
- [48] D.-P. Fan, W. Wang, M.-M. Cheng, and J. Shen, “Shifting more attention to video salient object detection,” in *Proceedings of the IEEE/CVF Conference on Computer Vision and Pattern Recognition*, 2019, pp. 8554–8564. 3, 9
- [49] K. Simonyan and A. Zisserman, “Very deep convolutional networks for large-scale image recognition,” *arXiv preprint arXiv:1409.1556*, 2014. 3, 6, 7
- [50] T.-Y. Lin, P. Dollár, R. Girshick, K. He, B. Hariharan, and S. Belongie, “Feature pyramid networks for object detection,” in *Proceedings of the IEEE conference on computer vision and pattern recognition*, 2017, pp. 2117–2125. 3
- [51] A. Goyal and Y. Bengio, “Inductive biases for deep learning of higher-level cognition,” *arXiv preprint arXiv:2011.15091*, 2020. 4
- [52] C. R. Qi, H. Su, K. Mo, and L. J. Guibas, “Pointnet: Deep learning on point sets for 3d classification and segmentation,” in *Proceedings of the IEEE conference on computer vision and pattern recognition*, 2017, pp. 652–660. 5
- [53] T. Park, M.-Y. Liu, T.-C. Wang, and J.-Y. Zhu, “Semantic image synthesis with spatially-adaptive normalization,” in *Proceedings of the IEEE/CVF conference on computer vision and pattern recognition*, 2019, pp. 2337–2346. 5
- [54] X. Qin, Z. Zhang, C. Huang, C. Gao, M. Dehghan, and M. Jagersand, “Basnet: Boundary-aware salient object detection,” in *Proceedings of the IEEE/CVF conference on computer vision and pattern recognition*, 2019, pp. 7479–7489. 5, 8
- [55] M. Everingham, S. Eslami, L. Van Gool, C. K. Williams, J. Winn, and A. Zisserman, “The pascal visual object classes challenge: A retrospective,” *International journal of computer vision*, vol. 111, no. 1, pp. 98–136, 2015. 5
- [56] D. Batra, A. Kowdle, D. Parikh, J. Luo, and T. Chen, “icoseg: Interactive co-segmentation with intelligent scribble guidance,” in *2010 IEEE computer society conference on computer vision and pattern recognition*. IEEE, 2010, pp. 3169–3176. 5
- [57] J. Shotton, J. Winn, C. Rother, and A. Criminisi, “Textonboost: Joint appearance, shape and context modeling for multi-class object recognition and segmentation,” in *European conference on computer vision*. Springer, 2006, pp. 1–15. 5
- [58] D. Zhang, J. Han, C. Li, and J. Wang, “Co-saliency detection via looking deep and wide,” in *Proceedings of the IEEE conference on computer vision and pattern recognition*, 2015, pp. 2994–3002. 5
- [59] D.-P. Fan, T. Li, Z. Lin, G.-P. Ji, D. Zhang, M.-M. Cheng, H. Fu, and J. Shen, “Re-thinking co-salient object detection,” *IEEE Transactions on Pattern Analysis and Machine Intelligence*, 2021. 5, 8
- [60] F. Perazzi, J. Pont-Tuset, B. McWilliams, L. Van Gool, M. Gross, and A. Sorkine-Hornung, “A benchmark dataset and evaluation methodology for video object segmentation,” in *Proceedings of the IEEE conference on computer vision and pattern recognition*, 2016, pp. 724–732. 5
- [61] P. Ochs, J. Malik, and T. Brox, “Segmentation of moving objects by long term video analysis,” *IEEE transactions on pattern analysis and machine intelligence*, vol. 36, no. 6, pp. 1187–1200, 2013. 5, 13
- [62] W. Wang, J. Shen, and L. Shao, “Consistent video saliency using local gradient flow optimization and global refinement,” *IEEE Transactions on Image Processing*, vol. 24, no. 11, pp. 4185–4196, 2015. 6, 13
- [63] F. Li, T. Kim, A. Humayun, D. Tsai, and J. M. Rehg, “Video segmentation by tracking many figure-ground segments,” in *Proceedings of the IEEE international conference on computer vision*, 2013, pp. 2192–2199. 6, 13
- [64] F. Perazzi, P. Krähenbühl, Y. Pritch, and A. Hornung, “Saliency filters: Contrast based filtering for salient region detection,” in *2012 IEEE conference on computer vision and pattern recognition*. IEEE, 2012, pp. 733–740. 6
- [65] R. Achanta, S. Hemami, F. Estrada, and S. Susstrunk, “Frequency-tuned salient region detection,” in *2009 IEEE conference on computer vision and pattern recognition*. IEEE, 2009, pp. 1597–1604. 6
- [66] D.-P. Fan, C. Gong, Y. Cao, B. Ren, M.-M. Cheng, and A. Borji, “Enhanced-alignment measure for binary foreground map evaluation,” *arXiv preprint arXiv:1805.10421*, 2018. 6
- [67] D.-P. Fan, M.-M. Cheng, Y. Liu, T. Li, and A. Borji, “Structure-measure: A new way to evaluate foreground maps,” in *Proceedings of the IEEE international conference on computer vision*, 2017, pp. 4548–4557. 6
- [68] D. P. Kingma and J. Ba, “Adam: A method for stochastic optimization,” *arXiv preprint arXiv:1412.6980*, 2014. 6
- [69] X. Wang, R. Girshick, A. Gupta, and K. He, “Non-local neural networks,” in *Proceedings of the IEEE conference on computer vision and pattern recognition*, 2018, pp. 7794–7803. 6, 7
- [70] K. R. Jerripothula, J. Cai, and J. Yuan, “Image co-segmentation via saliency co-fusion,” *IEEE Transactions on Multimedia*, vol. 18, no. 9, pp. 1896–1909, 2016. 7
- [71] K. R. Jerripothula, J. Cai, J. Lu, and J. Yuan, “Object co-skeletonization with co-segmentation,” in *2017 IEEE Conference on Computer Vision and Pattern Recognition (CVPR)*. IEEE, 2017, pp. 3881–3889. 7
- [72] C. Wang, H. Zhang, L. Yang, X. Cao, and H. Xiong, “Multiple semantic matching on augmented  $n$ -partite graph for object co-segmentation,” *IEEE Transactions on Image Processing*, vol. 26, no. 12, pp. 5825–5839, 2017. 7
- [73] K.-J. Hsu, Y.-Y. Lin, Y.-Y. Chuang *et al.*, “Co-attention cnns for unsupervised object co-segmentation,” in *IJCAI*, vol. 1, 2018, p. 2. 7
- [74] J.-J. Liu, Q. Hou, M.-M. Cheng, J. Feng, and J. Jiang, “A simple pooling-based design for real-time salient object detection,” in *Proceedings of the IEEE/CVF conference on computer vision and pattern recognition*, 2019, pp. 3917–3926. 8
- [75] J.-X. Zhao, J.-J. Liu, D.-P. Fan, Y. Cao, J. Yang, and M.-M. Cheng, “Egnet: Edge guidance network for salient object detection,” in *Proceedings of the IEEE/CVF international conference on computer vision*, 2019, pp. 8779–8788. 8
- [76] Z. Wu, L. Su, and Q. Huang, “Stacked cross refinement network for edge-aware salient object detection,” in *Proceedings of the IEEE/CVF international conference on computer vision*, 2019, pp. 7264–7273. 8
- [77] B. Li, Z. Sun, L. Tang, Y. Sun, and J. Shi, “Detecting robust co-saliency with recurrent co-attention neural network,” in *IJCAI*, vol. 2, 2019, p. 6. 8
- [78] K. Zhang, T. Li, B. Liu, and Q. Liu, “Co-saliency detection via mask-guided fully convolutional networks with multi-scale label smoothing,” in *Proceedings of the IEEE/CVF Conference on Computer Vision and Pattern Recognition*, 2019, pp. 3095–3104. 8
- [79] Y. Chen, W. Zou, Y. Tang, X. Li, C. Xu, and N. Komodakis, “Scom: Spatiotemporal constrained optimization for salient object detection,” *IEEE Transactions on Image Processing*, vol. 27, no. 7, pp. 3345–3357, 2018. 9
- [80] G. Li and Y. Yu, “Deep contrast learning for salient object detection,” in *Proceedings of the IEEE conference on computer vision and pattern recognition*, 2016, pp. 478–487. 9
- [81] S. Li, B. Seybold, A. Vorobyov, X. Lei, and C.-C. J. Kuo, “Unsupervised video object segmentation with motion-based bilateral networks,” in *Proceedings of the European conference on computer vision (ECCV)*, 2018, pp. 207–223. 9
- [82] H. Song, W. Wang, S. Zhao, J. Shen, and K.-M. Lam, “Pyramid dilated deeper convlstm for video salient object detection,” in *Proceedings of the European conference on computer vision (ECCV)*, 2018, pp. 715–731. 9
- [83] R. Cong, J. Lei, H. Fu, F. Porikli, Q. Huang, and C. Hou, “Video saliency detection via sparsity-based reconstruction and propagation,” *IEEE Transactions on Image Processing*, vol. 28, no. 10, pp. 4819–4831, 2019. 9

- [84] C. Chen, G. Wang, C. Peng, X. Zhang, and H. Qin, "Improved robust video saliency detection based on long-term spatial-temporal information," *IEEE transactions on image processing*, vol. 29, pp. 1090–1100, 2019. [9](#)
- [85] Y. Ji, H. Zhang, Z. Jie, L. Ma, and Q. J. Wu, "Casnet: A cross-attention siamese network for video salient object detection," *IEEE transactions on neural networks and learning systems*, vol. 32, no. 6, pp. 2676–2690, 2020. [9](#)
- [86] M. Zhen, S. Li, L. Zhou, J. Shang, H. Feng, T. Fang, and L. Quan, "Learning discriminative feature with crf for unsupervised video object segmentation," in *European Conference on Computer Vision*. Springer, 2020, pp. 445–462. [9](#)
- [87] H. Park, J. Yoo, S. Jeong, G. Venkatesh, and N. Kwak, "Learning dynamic network using a reuse gate function in semi-supervised video object segmentation," in *Proceedings of the IEEE/CVF Conference on Computer Vision and Pattern Recognition*, 2021, pp. 8405–8414. [8](#), [9](#)
- [88] J. Mei, M. Wang, Y. Lin, Y. Yuan, and Y. Liu, "Transvos: Video object segmentation with transformers," *arXiv preprint arXiv:2106.00588*, 2021. [8](#), [9](#)
- [89] K. He, X. Zhang, S. Ren, and J. Sun, "Deep residual learning for image recognition," in *Proceedings of the IEEE conference on computer vision and pattern recognition*, 2016, pp. 770–778. [9](#)
- [90] A. Howard, M. Sandler, G. Chu, L.-C. Chen, B. Chen, M. Tan, W. Wang, Y. Zhu, R. Pang, V. Vasudevan *et al.*, "Searching for mobilenetv3," in *Proceedings of the IEEE/CVF International Conference on Computer Vision*, 2019, pp. 1314–1324. [9](#)
- [91] J. Pont-Tuset, F. Perazzi, S. Caelles, P. Arbeláez, A. Sorkine-Hornung, and L. Van Gool, "The 2017 davis challenge on video object segmentation," *arXiv preprint arXiv:1704.00675*, 2017. [9](#)
- [92] N. Xu, L. Yang, Y. Fan, D. Yue, Y. Liang, J. Yang, and T. Huang, "Youtube-vos: A large-scale video object segmentation benchmark," *arXiv preprint arXiv:1809.03327*, 2018. [9](#), [14](#)
- [93] T. Liu, Z. Yuan, J. Sun, J. Wang, N. Zheng, X. Tang, and H.-Y. Shum, "Learning to detect a salient object," *IEEE Transactions on Pattern analysis and machine intelligence*, vol. 33, no. 2, pp. 353–367, 2010. [8](#), [13](#)
- [94] K. Sun, B. Xiao, D. Liu, and J. Wang, "Deep high-resolution representation learning for human pose estimation," in *Proceedings of the IEEE/CVF Conference on Computer Vision and Pattern Recognition*, 2019, pp. 5693–5703. [13](#)
- [95] C. Wah, S. Branson, P. Welinder, P. Perona, and S. Belongie, "The caltech-ucsd birds-200-2011 dataset," 2011. [14](#)
- [96] K. Tang, A. Joulin, L.-J. Li, and L. Fei-Fei, "Co-localization in real-world images," in *Proceedings of the IEEE conference on computer vision and pattern recognition*, 2014, pp. 1464–1471. [14](#)
- [97] G. Bradski, "The opencv library," *Dr. Dobb's Journal: Software Tools for the Professional Programmer*, vol. 25, no. 11, pp. 120–123, 2000. [14](#)

## Supplementary Material

This supplementary material contains more details of the network, including the details of using optical flow, more training details, more analysis, more downstream applications and more additional qualitative results in our paper “A Unified Transformer Framework for Group-based Segmentation: Co-Segmentation, Co-Saliency Detection and Video Salient Object Detection”.

### A. Details of Using Optical Flow

As we have discussed in our main paper, optical flow is optional to add into our network, and applying flow cues to our network is straightforward. First of all, let us first introduce why optical flow can help us. As is shown in Fig 8, when we directly use the optical flow as input, the output predictions are comparable. This is because the optical flows reflect the foreground moving salient objects without any complicated backgrounds, and thus, our network can well extract their features and yields the masks. Based on this, we consider that combining the optical flow features with the origin image feature can help the network focus on more foreground salient objects. Fig 9 shows us the overall architecture of using the optical flow information. Specifically, we maintain the transformer block, intra-MLP learning module, and decoder unchanged but slightly modify the encoder features. We take both the optical flows generated by FlowNet2.0 [24] and adjacent frames as input, and they share the same encoder. The enhanced features of the group-based images to be fed into the subsequent network can be formulated as:

$$\begin{aligned} F_{3\_img} &= F_{3\_flow} \times F_{3\_img}, \\ F_{4\_img} &= F_{4\_flow} \times F_{4\_img}. \end{aligned} \quad (8)$$

This operation enables the image features to pay more attention to the targeted regions by combining flow cues regardless of the distracting background items. Note that our method of using optical flow may not be the optimal way, maybe using a separate optical flow branch and a unique combination can further improve the network performance. However, using the optical flow is not our framework’s main purpose and contribution, we can already achieve state-of-the-art performance on three benchmarks (*i.e.*, FBMS [61], ViSal [62] and SegV2 [63]) without using it. We will continue to refine and research possible ways to improve our network in future work.

### B. More Training Details

For object co-segmentation (CoS) and co-saliency detection (CoSD), unlike the previous methods (*i.e.*, GCAGC [18], CADC [13]) that are trained on both COCO-SEG [14] and other saliency datasets (*i.e.*, MSRA-B [93], DUTS [15]), we train our method only using COCO-SEG [14] dataset and without using data augmentation like copy-and-paste in CADC [13], Jigsaw in GICD [34]. For video salient object detection (VSOD), we follow the previous works (*i.e.*, FSNet [11], PCSA [10]) that employ the random flip, random rotation and multi-scale  $\{0.75, 1, 1.25\}$  training strategy in the training phase.

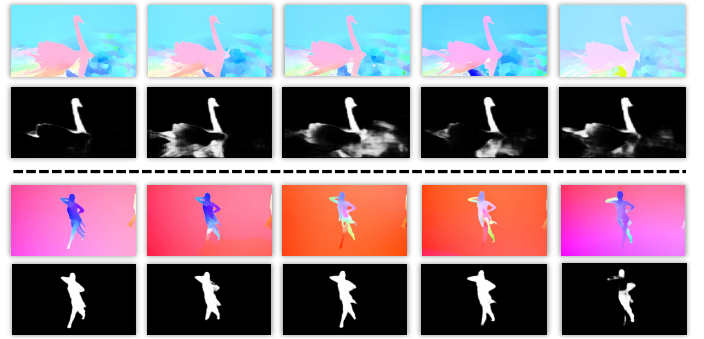


Fig. 8: The predictions of the direct optical flow input.

Method	PASCAL		iCoseg	
	$\mathcal{P}$	$\mathcal{J}$	$\mathcal{P}$	$\mathcal{J}$
$K = 2$	94.5	72.8	97.1	90.2
$K = 4$	<b>95.4</b>	<b>73.6</b>	<b>97.6</b>	<b>90.9</b>
$K = 6$	95.2	73.3	97.5	90.6

TABLE IX: Analysis of the  $K$  number in intra-MLP learning module.

Method	PASCAL		iCoseg	
	$\mathcal{P}$	$\mathcal{J}$	$\mathcal{P}$	$\mathcal{J}$
$D = 512$	94.7	72.3	96.5	89.5
$D = 782$	<b>95.4</b>	<b>73.6</b>	<b>97.6</b>	<b>90.9</b>
$D = 1024$	94.9	73.1	97.0	90.3

TABLE X: Analysis of the dim channel in transformer projection function.

### C. More Analysis

**The number of  $K$ .** We here explore the effect of the  $K$  number we use in the intra-MLP learning module. As shown in Tab IX, we find that when  $K = 4$ , our network can achieve the best performance. We conjecture that a small or too large  $K$  number may make the network learn less useful corresponding semantic information or redundant information that harms the network.

**The Dim Channels.** We further conduct an additional experiment to analyze the effect of the dim channel in our transformer block projection function. Since the top-level output features map channels are 512, and thus, we explore  $\{D = 512, 782, 1024\}$ , respectively. Tab X shows that when  $D = 782$  the network performs the best. Note that keep enlarging the dim channel will not only bring no gain to the network, but also consume computing resources.

**Stronger Backbone.** Furthermore, we adopt a stronger backbone HRNet [94] to conduct experiments on VSOD tasks, whose results are shown in Tab XI. Although using a more powerful backbone can improve the performance of the network, the execution time will also increase at the same time. As we mentioned in our main paper, using vgg16 backbone can already achieve the state-of-the-art performance and the execution speed can also reach real-time. Therefore, we recommend

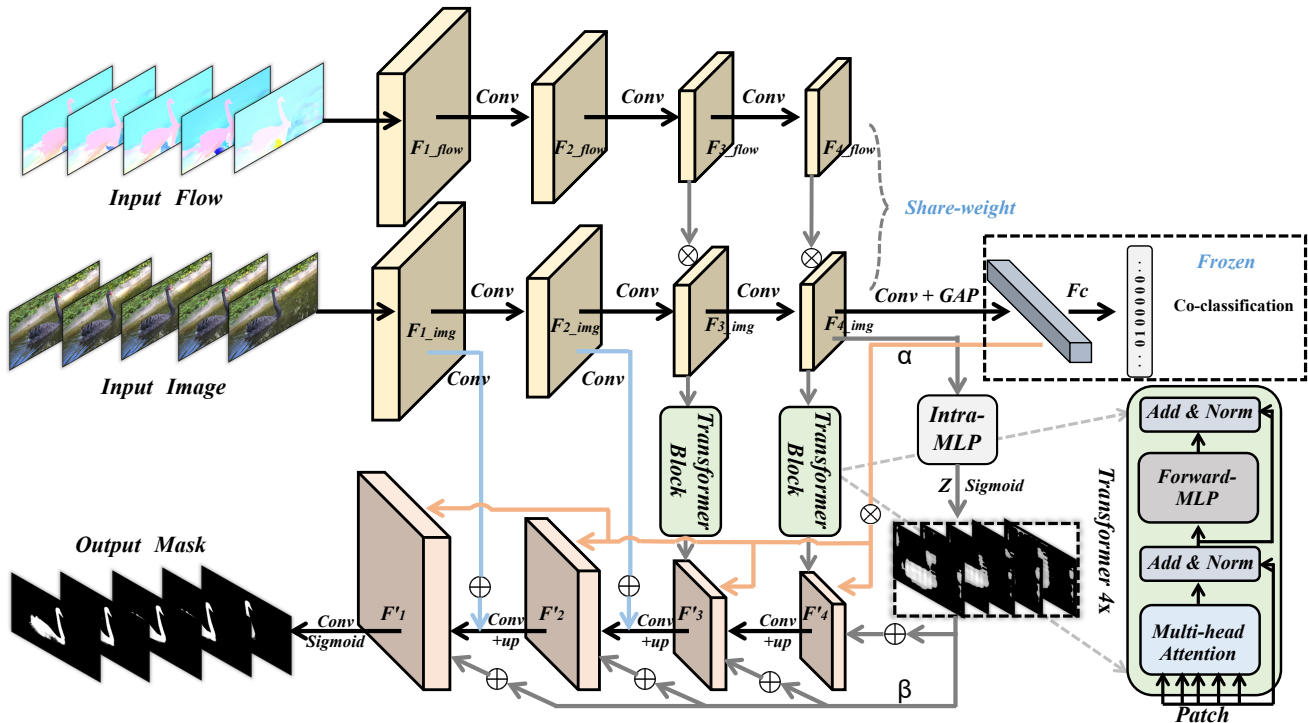


Fig. 9: The overall architecture of combining the optical flow information.

Method	Setting	OF	Sup	RT	DAVIS <sub>16</sub>			FBMS			ViSal			SegV2		
					MAE↓	S <sub>m</sub> ↑	F <sub>β</sub> ↑	MAE↓	S <sub>m</sub> ↑	F <sub>β</sub> ↑	MAE↓	S <sub>m</sub> ↑	F <sub>β</sub> ↑	MAE↓	S <sub>m</sub> ↑	F <sub>β</sub> ↑
UFO (Ours)	HRNet-224	✗	U	0.01	0.028	0.881	0.842	0.026	0.899	0.893	0.012	0.958	0.948	0.018	0.897	0.866
UFO (Ours)	HRNet-224	✓	U	0.03	0.013	0.921	0.907	0.033	0.888	0.887	0.011	0.962	0.956	0.012	0.901	0.867

TABLE XI: *OF* denotes the optical flow. *RT* denotes the runtime (s). “U”: unsupervised method. The number behind the backbone is the input resolution.

using vgg16, which can already meet most of the needs in our tasks.

#### D. More Downstream Applications

**Co-Localization.** We try to conduct an additional experiment on CUB-2011 [95] dataset for co-localization task, which is also aims to simultaneously localize objects of the same class across a set of distinct images [96]. As shown in Fig 11, we first generate the object masks on the co-objects. Then, we obtain the green predated box according to the binary masks. As can be seen, our predicted bounding boxes are closed to the GT bounding boxes.

**Real-Time Video Salient Object Detection.** Our framework can be applied to detect the salient object in the video without using optical flow, therefore, it can be easily to conduct this task. We use a video sample from the public website<sup>1</sup> for our demo. The result are provided in our publicly released code page. Note that we do not train our network on YouTube-VOS [92] dataset, and the competitive result of the randomly selected demo video shows the superiority of our proposed method.



Fig. 10: Visualizations of object matching flow.

**Bullet-Chat Blocking.** Bullet-chat blocking aims to prevent the salient objects in the video from being occluded by the viewer’s barrage. It has to segment out the object and yield a accurate mask that provides to block the bullet-chat text in the foreground. To validate the generality of our method, we use a video sample from the public website<sup>2</sup>. And then we adopt the OpenCV [97] toolbox to generate some pseudo bullet-chat that constantly slides over the video. Finally, we can produce a new bullet-chat blocking video as we provide in our publicly released code page.

<sup>1</sup><https://www.youtube.com/watch?v=aSqeWUuQSIM&t=1s>

<sup>2</sup><https://www.youtube.com/watch?v=kpUYkG0FAYk&t=146s>

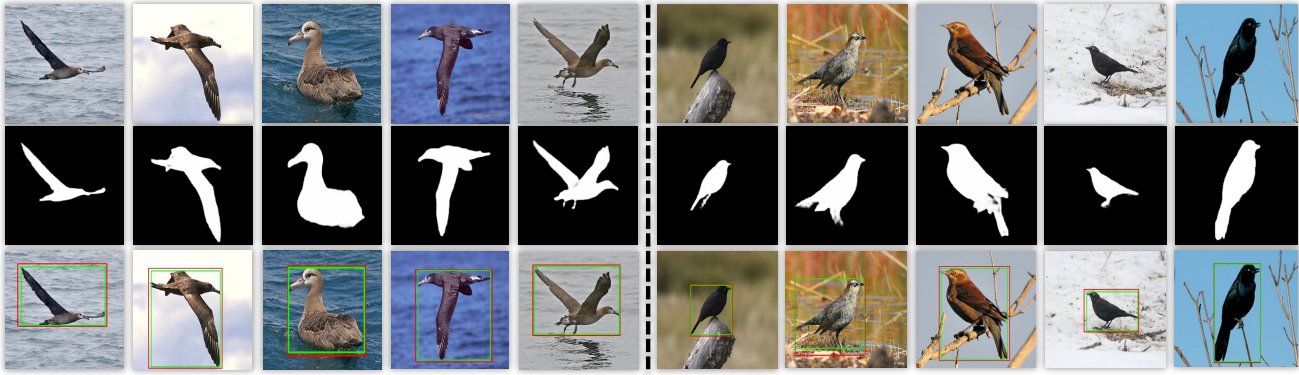


Fig. 11: **Visualizations of co-localization.** The 1<sup>st</sup> row are the input images, the 2<sup>nd</sup> row are our predicted masks, and the 3<sup>rd</sup> row are the localization results. The ground-truth bounding box is in red and predicted bounding box is green.

### E. More Visualizations

**Matching.** To further provide the network interpretability, we visualize how group-based images match features with each other during network learning. Fig 10 shows the highly correlated patches in different images, which illustrates that our network can well capture the object similarities and discover the object regions.

**Co-Segmentation.** Fig 12 shows more visualizations on CoS task.

**Co-Saliency Detection.** Fig 13 shows more visualizations on CoSD tasks.

**Video Salient Object Detection.** Fig 14 shows more visualizations on VSOD tasks.

Note that all the predicted results can be found and downloaded in our project page: <https://github.com/suyukun666/UFO>.

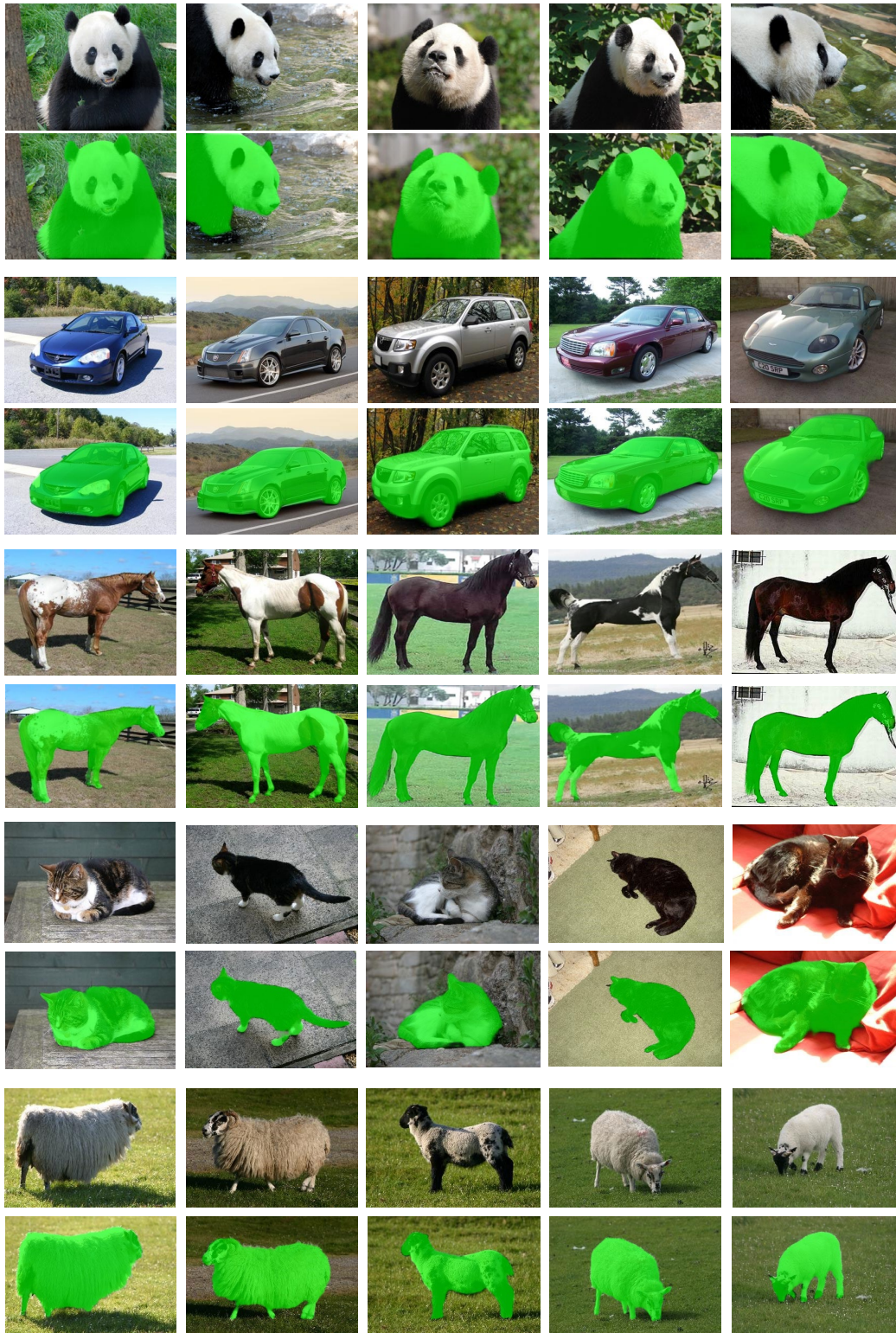


Fig. 12: Visualizations of co-segmentation.

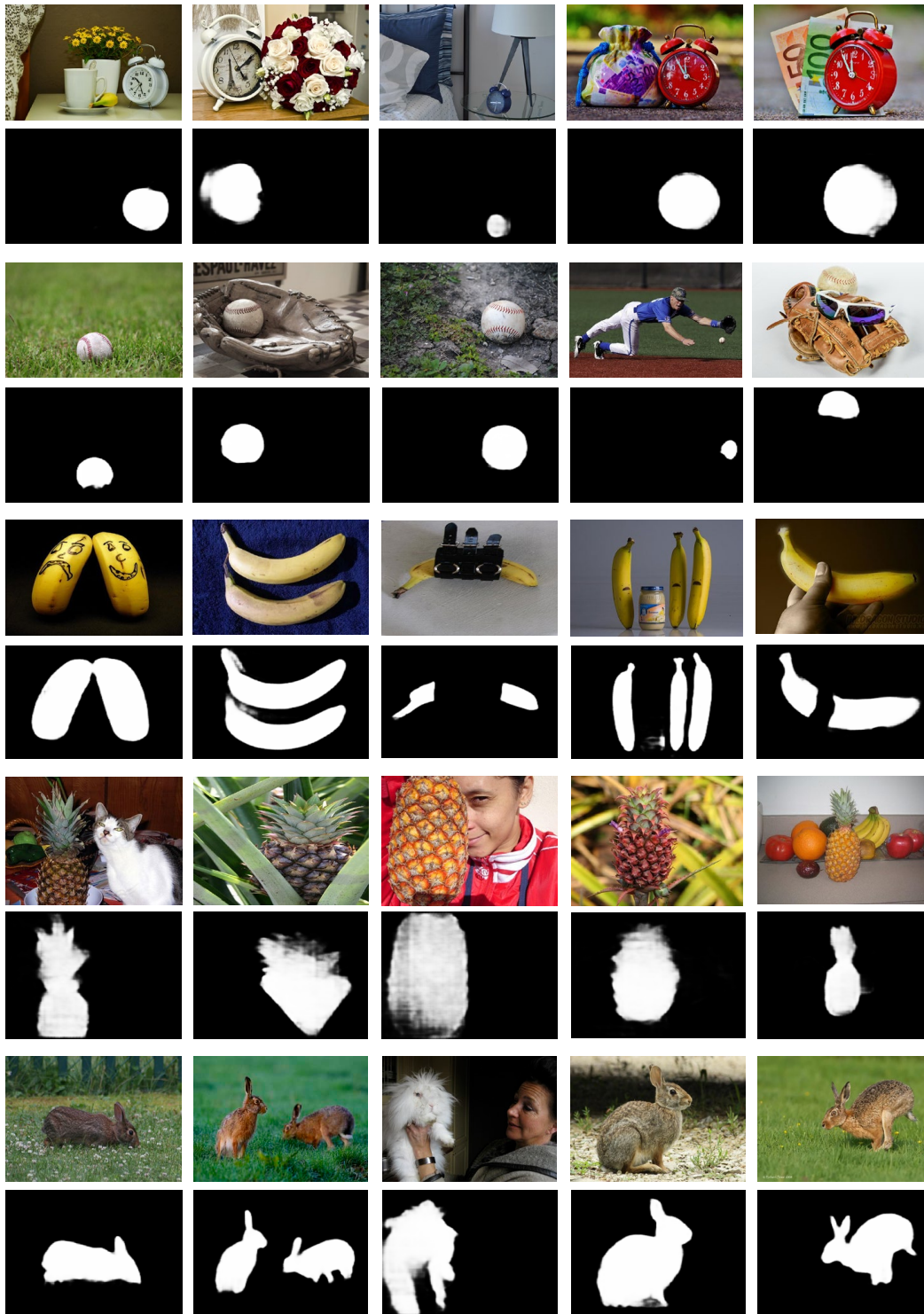


Fig. 13: Visualizations of co-saliency detection.

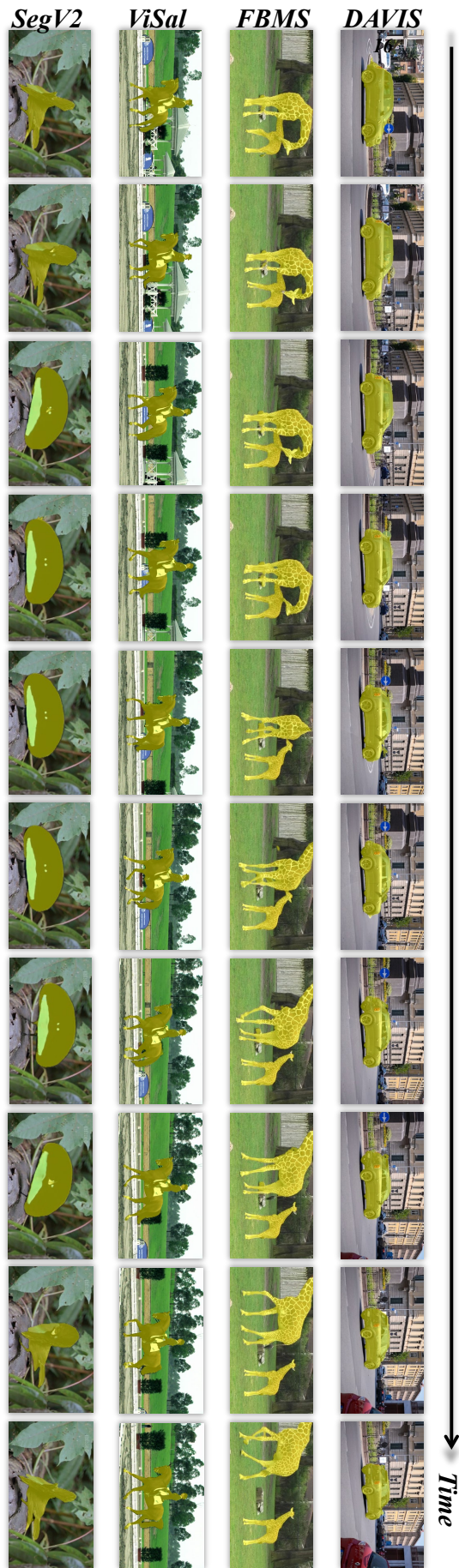


Fig. 14: Visualizations of video salient object detection.